Atmospheric
Chemistry
and Physics

Estimates of black carbon emissions in the western United States using the GEOS-Chem adjoint model

Y. H. Mao[1,2,3], Q. B. Li[1,2], D. K. Henze[4], Z. Jiang[5,a], D. B. A. Jones[5,2], M. Kopacz[6], C. He[1,2], L. Qi[1,2], M. Gao[1,2], W.-M. Hao[7], and K.-N. Liou[1,2]

[1]Department of Atmospheric and Oceanic Sciences, University of California, Los Angeles, CA 90095, USA
[2]Joint Institute for Regional Earth System Science and Engineering, University of California, Los Angeles, CA 90095, USA
[3]State Key Laboratory of Atmospheric Boundary Layer Physics and Atmospheric Chemistry,
Institute of Atmospheric Physics, Chinese Academy of Sciences, Beijing, 100029, China
[4]Department of Mechanical Engineering, University of Colorado, Boulder, CO 80309, USA
[5]Department of Physics, University of Toronto, Toronto, ON M5S 1A7, Canada
[6]NOAA Climate Program Office, Silver Spring, Maryland, 20910, USA
[7]Fire Sciences Laboratory, U.S. Forest Service, Missoula, MT, 59808, USA
[a]now at: Jet Propulsion Laboratory, California Institute of Technology, Pasadena, CA, 91109, USA

Correspondence to: Q. B. Li (qli@atmos.ucla.edu)

Abstract. We estimate black carbon (BC) emissions in the western United States for July–September 2006 by inverting surface BC concentrations from the Interagency Monitoring of Protected Visual Environments (IMPROVE) network using a global chemical transport model (GEOS-Chem) and its adjoint. Our best estimate of the BC emissions is 49.9 Gg at $2° \times 2.5°$ (a factor of 2.1 increase) and 47.3 Gg at $0.5° \times 0.667°$ (1.9 times increase). Model results now capture the observed major fire episodes with substantial bias reductions ($\sim 35\%$ at $2° \times 2.5°$ and $\sim 15\%$ at $0.5° \times 0.667°$). The emissions are ~ 20–50% larger than those from our earlier analytical inversions (Mao et al., 2014). The discrepancy is especially drastic in the partitioning of anthropogenic versus biomass burning emissions. The August biomass burning BC emissions are 4.6–6.5 Gg and anthropogenic BC emissions 8.6–12.8 Gg, varying with the model resolution, error specifications, and subsets of observations used. On average both anthropogenic and biomass burning emissions in the adjoint inversions increase 2-fold relative to the respective a priori emissions, in distinct contrast to the halving of the anthropogenic and tripling of the biomass burning emissions in the analytical inversions. We attribute these discrepancies to the inability of the adjoint inversion system, with limited spatiotemporal coverage of the IMPROVE observations, to effectively distinguish collocated anthropogenic and biomass burning emissions on model grid scales. This calls for concurrent measurements of other tracers of biomass burning and fossil fuel combustion (e.g., carbon monoxide and carbon isotopes). We find that the adjoint inversion system as is has sufficient information content to constrain the total emissions of BC on the model grid scales.

1 Introduction

Black carbon (BC) is directly emitted from the incomplete combustion of carbonaceous fuels (Bond et al., 2004). Black carbon has substantial impacts on global climate because of its strong absorption of solar radiation (e.g., Horvath, 1993; Ramanathan and Carmichael, 2008), important influences in cloud processes (Jacobson, 2006), and significant impacts on snow and ice albedos (Flanner et al., 2007, 2009). The radiative forcing due to BC is 0.64 W m^{-2} globally (IPCC, 2013), ranked as the third-biggest human cause of global warming. Black carbon is also known as an important agent to both degrade air quality and affect human health (McMurry et al., 2004; Anenberg et al., 2011, 2012). Because of its shorter lifetime relative to long-lived greenhouse gases, BC reduc-

tion may provide an efficient near-term solution to mitigate global warming and to improve air quality and public health simultaneously (Ramanathan and Carmichael, 2008; Shindell et al., 2008, 2012; Smith et al., 2009; Ramana et al., 2010; Bond et al., 2013).

The deposition of BC on glaciers is known to be an important driver to the observed rapid glacier retreat (Xu et al., 2009; Painter et al., 2013) and further impacts the regional hydrological cycle over mountain ranges (Qian et al., 2009). In the western United States (WUS), mountain snowmelt accounts for at least 70 % of the annual stream flow (Qian et al., 2009). In the recent decades, the WUS is experiencing the most severe drought (e.g., Melillo et al., 2014) and the water level of the Colorado River has been decreasing (e.g., Vano et al., 2013). It is thus imperative to better understand the sources, transport, and deposition of BC in the WUS mountain ranges.

Recent studies have shown that the biomass burning BC emissions in the WUS were underestimated by a factor of 2 in both the absolute magnitudes and the timing and location of the emissions (Mao et al., 2011, and references therein). The large uncertainty is partially because previous burned area algorithms lacked the ability to detect small fires (Giglio et al., 2010; Randerson et al., 2012). Long-term records have shown an increase in fires in terms of both fire frequency and burned area in the WUS over the past 30 years because of the rising spring and summer temperatures (Westerling et al., 2006; Peterson and Marcinkowski, 2014; Jin et al., 2014) and increasing urbanization (e.g., Cannon and DeGraff, 2009). This upward trend is expected to continue as a result of the warming climate (Spracklen et al., 2009; Yue et al., 2013). Biomass burning emissions will conceivably have an even larger contribution to BC in the WUS in this century, especially considering that North American anthropogenic emissions have been steadily decreasing as a result of effective emission controls (Novakov et al., 2003; Bond et al., 2007; Ramanathan and Carmichael, 2008).

Knowledge of the emissions of a chemical species is imperative for better understanding of its transport, distribution, and removal. Traditional bottom-up emission estimates generally depend on emission factors using socioeconomic, energy, land use, or environmental data (Bond et al., 2007, 2013; Lu et al., 2011). Inverse modeling is able to improve the bottom-up emission estimates by minimizing an error-weighted least squares cost function (Rodgers, 2000). There are two methods to achieve the minimum of the cost function, the so-called analytical inversion and adjoint (i.e., variational) inversion (Kopacz et al., 2009, and references therein). The analytical method obtains an analytical solution by explicitly constructing a Jacobian matrix. However, the analytical method limits the number of the observations and the number of the sources and source regions that could be optimized because it is computationally expensive. Alternatively, the adjoint method seeks a numerical solution iteratively by using a suitable optimization algorithm (e.g., the

conjugate gradient method) and is thus able to handle a very large number of observations and a large state vector resolved on a model grid scale.

Inverse modeling in general is suited for estimating emissions of unreactive or weakly reactive chemical species when their atmospheric concentrations are linearly or weakly non-linearly dependent on emissions (Müller and Stavrakou, 2005). These species include but are not limited to carbon dioxide (e.g., Gloor et al., 1999; Chevallier et al., 2007; Pickett-Heaps et al., 2011), methane (e.g., Hein et al., 1997; Meirink et al., 2008; Wecht et al., 2012), and carbon monoxide (CO) (Stavrakou and Müller, 2006; Arellano et al., 2004, 2006, 2007; Chevallier et al., 2009; Jones et al., 2009; Jiang et al., 2013). Despite the non-linear complexities of the inversion system for short-lived tracer species, several studies have attempted to constrain emissions for nitrogen oxides (e.g., Martin et al., 2003, 2006; Chai et al., 2009; Lin et al., 2010; Zyrichidou et al., 2013), sulfur dioxide (Lee et al., 2011), and ammonia (Zhu et al., 2013; Paulot et al., 2014). The inverse method has also been used to constrain emission fluxes of aerosols, for instance, inorganic particulate matter (Henze et al., 2009; Xu et al., 2013) and dust (Yumimoto et al., 2008; Wang et al., 2012).

A number of modeling studies have attempted to constrain and attribute BC emissions on regional to continental scales. Several studies have used multiple regressions to estimate annual mean emissions of primary carbonaceous aerosols in the US (Park et al., 2003) and in China (Fu et al., 2012; Wang et al., 2013). A global chemical transport model (CTM) and its adjoint was used to attribute the source regions of BC in the Himalayas and the Tibetan Plateau (Kopacz et al., 2011). Anthropogenic and biomass burning emissions of BC during the Asian Pacific Regional Aerosol Characterization Experiment (ACE-Asia) (Huebert et al., 2003; Seinfeld et al., 2004) were estimated using a continental-scale CTM (stretched over the Pacific basin) and its adjoint (Hakami et al., 2005). Previously, linear analytical inversions were applied to optimize sources and source regions (the Rockies, California and the Southwest, and the Pacific Northwest) of BC in the WUS for May–October 2006 (Mao et al., 2014). The analytical inversions show a factor of 3–5 increase of the biomass burning emissions and a ~ 50 % reduction of the anthropogenic emissions, relative to the corresponding a priori (Mao et al., 2014).

Here we apply the adjoint inversion method (Henze et al., 2007, 2009) to improve estimates of BC emissions in the WUS (defined hereinafter as 30–50° N, 100–125° W) on model grid scales by inverting the surface BC concentrations from the Interagency Monitoring of Protected Visual Environments (IMPROVE, Malm et al., 1994) network using the GEOS-Chem global 3-D CTM and its adjoint. We use the observations for 2006 from 69 mostly mountainous sites in the WUS (Fig. 1). We focus our analysis on biomass burning emissions during the large fire season of July–September in the region (Mao et al., 2011, 2014).

Table 1. Monthly biomass burning and anthropogenic emissions of BC (unit: Gg) in the WUS for August 2006.

		Inversion configurations					Emissions[a] (Gg (10^9 g))					
		Model	Site	S_aBB	S_aAnth	S_Σ	A priori	Biomass burning				Anth.	Total
		Resolution	num.	(%)	(%)	(%)	BB.	RM	CSW	PNW	Total		
A priori								1.3	0.5	1.0	2.8	5.8	8.6
A posteriori	Analytical	$2° \times 2.5°$	69	500	50	30	2.8	7.6	1.4	0.9	9.9 (3.5[b])	2.8 (0.5)	12.7 (1.5)
		$0.5° \times 0.667°$	69	500	50	30	2.8	4.1	0.1	1.9	6.1 (2.7)	3.1 (0.5)	9.1 (1.1)
	Adjoint	Case 1 $\quad 2° \times 2.5°$	69	500	50	30	2.8	3.0	1.4	1.5	5.9 (2.1)	11.8 (2.0)	17.7 (2.1)
		Case 2 $\quad 2° \times 2.5°$	69	300	50	30	2.8	2.9	1.3	1.4	5.6 (2.0)	11.6 (2.0)	17.2 (2.0)
		Case 3 $\quad 2° \times 2.5°$	69	500	30	30	2.8	3.2	1.4	1.6	6.2 (2.2)	11.4 (2.0)	17.6 (2.0)
		Case 4 $\quad 2° \times 2.5°$	69	500	200	30	2.8	3.3	1.5	1.7	6.5 (2.3)	12.8 (2.2)	19.3 (2.2)
		Case 5 $\quad 2° \times 2.5°$	69	500	50	100	2.8	2.4	1.2	1.0	4.6 (1.7)	10.3 (1.8)	14.9 (1.7)
		Case 6 $\quad 2° \times 2.5°$	56	500	50	30	2.8	2.8	1.3	1.4	5.5 (2.0)	11.1 (1.9)	16.6 (1.9)
		Case 7 $\quad 2° \times 2.5°$	69	200	200	30	2.8	3.1	1.4	1.5	6.0 (2.2)	12.5 (2.2)	18.5 (2.2)
		Case 8 $\quad 2° \times 2.5°$	69	500	50	30	3.0[c]	3.1	1.4	1.5	6.0 (2.1)	11.6 (2.0)	17.6 (2.0)
		Case 9 $\quad 0.5° \times 0.667°$	69	500	50	30	2.8	2.2	0.8	2.3	5.3 (1.9)	8.6 (1.5)	13.9 (1.6)

[a] See Fig. 1 in Mao et al. (2014) for the geographical definitions of the BC source regions. [b] Scaling factors are in parentheses. [c] The a priori biomass burning emissions uniformly increased by 2.5 Mg in every model grid box.
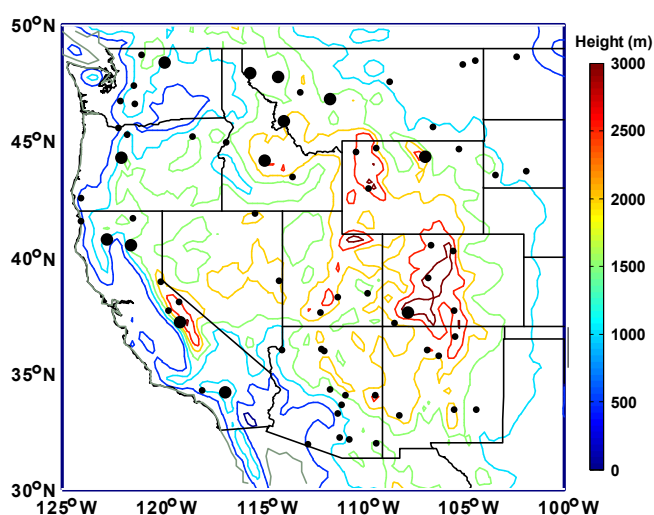

Figure 1. IMPROVE sites (data available at http://vista.cira.colostate.edu/improve/; solid circles) in the western United States (WUS). We use all the 69 sites in the standard inversion Case 1 (Table 1). Small 56 solid circles represent the sites used in the inversion Case 6 (Table 1). Also shown are terrain heights (color contours).

2 GEOS-Chem and its adjoint

We apply the GEOS-Chem global 3-D CTM (Bey et al., 2001; with many updates thenceforth) to analyze IMPROVE BC data. Here we use GEOS-Chem version 8-02-01 (available at http://geos-chem.org) driven by GEOS-5 meteorological data. The detailed model configurations are as discussed by Mao et al. (2011, 2014). Global annual anthropogenic emissions of BC are from Bond et al. (2007). Seasonal variations of anthropogenic emissions are considered over the US following Park et al. (2003). Biomass burning emissions of BC are from the Global Fire Emissions Database version 2 (GFEDv2) (Randerson et al., 2007; van

der Werf et al., 2006), with improved spatiotemporal distributions using the active fire counts from the Moderate Resolution Imaging Spectroradiometer (MODIS) (Mao et al., 2014). For computational expediency, we conduct "offline" simulations of carbonaceous aerosols (Mao et al., 2011, and references therein) for 2006 at both $2° \times 2.5°$ (globally) and $0.5° \times 0.667°$ (nested over North America, 40–140° W longitudes, 10–70° N latitudes, cf. Fig. 1 in Wang et al., 2004) horizontal resolutions, following Mao et al. (2014). The first 3 months are used for initialization, and we focus our analysis on July–September. Model results are sampled at the corresponding location and time of IMPROVE observations.

We use the GEOS-Chem adjoint (Henze et al., 2007, 2009) to estimate BC emissions in the WUS. A particular type of application of the adjoint is source attribution of chemical species at individual sites (e.g., Zhang et al., 2009; Kopacz et al., 2011; Parrington et al., 2012; Walker et al., 2012). Here we use the adjoint of the "offline" simulation of BC at $2° \times 2.5°$ (globally) and $0.5° \times 0.667°$ (nested over North America, Jiang et al., 2015a). The computational cost of the adjoint simulation is 50 % greater than that of the corresponding forward simulation. We validate the adjoint simulation of BC by comparing the adjoint gradients and the forward model sensitivities calculated using finite difference approximation (Henze et al., 2007; Zhu et al., 2013):

$$\wedge = \frac{J(\sigma + \delta\sigma) - J(\sigma)}{\delta\sigma}, \tag{1}$$

where J is the cost function (Mao et al., 2014, and references therein), as discussed below in Sect. 3.1, and σ the scaling factor of BC emissions. We use here $\delta\sigma = 0.1$, following Henze et al. (2007). Specifically we calculate the sensitivity of the BC mass at the surface with respect to the scaling factors of biomass burning and anthropogenic emissions of BC. Figure S1 in the Supplement shows the results from 1 week simulations for biomass burning (top panel) and anthropogenic emissions (bottom panel) for August 2006.

The adjoint and finite difference sensitivities are in excellent agreements ($r \approx 1$), reaffirming the accuracy of the adjoint code.

3 Inversion approach

3.1 The adjoint solution to the inverse problem

Consider the general problem of inferring emissions (state vector X) from a set of given observations (observation vector Y) with error ε. They are related via a forward model F as follows (Rodgers, 2000):

$$Y = F(X, b) + \varepsilon, \tag{2}$$

where X are the monthly biomass burning or anthropogenic emissions of BC in each model grid box in the present study, Y the 24 h average surface BC concentrations from the 69 IMPROVE sites (Fig. 1), b the model variables not directly retrieved from the inversion, F the GEOS-Chem model, and ε the observation error (measurement and forward model errors). Based on Bayes' theorem and the assumption of Gaussian error distributions (Rodgers, 2000), the optimal or maximum a posteriori (MAP) solution for X given Y is equivalent to finding the minimum of a cost function $J(X)$:

$$
\begin{aligned}
J(X) = &\frac{1}{2}\gamma_{\mathrm{r}}(X - X_{\mathrm{a}})^{\mathrm{T}}S_{\mathrm{a}}^{-1}(X - X_{\mathrm{a}}) + \\
&\frac{1}{2}\sum_{i=0}^{N}[Y_i - F(X_i)]^{\mathrm{T}}\mathbf{S}_{\varepsilon}^{-1}[Y_i - F(X_i)] \\
&= \gamma_{\mathrm{r}}J_{\mathrm{b}} + J_{\mathrm{o}},
\end{aligned}
\tag{3}
$$

where X_{a} and S_{a} are the a priori emissions and the associated error covariance, S_{ε} the observational error covariance, and γ_{r} the regularization parameter that adjusts the relative constraints by the observation term (i.e., the prediction term, J_{o}) and the background term (i.e., the penalty term, J_{b}) of the cost function (Hakami et al., 2005; Müller and Stavrakou, 2005; Henze et al., 2007; Kopacz et al., 2009). An observation term is added to the cost function for each additional data source during the time interval $[t_0, t_N]$.

The adjoint approach seeks to minimize the cost function $J(X)$ numerically and iteratively rather than analytically (Henze et al., 2007, 2009). Starting from an initial guess (i.e., the a priori emissions), the adjoint model efficiently computes the cost function gradients. A quasi-Newton L-BFGS algorithm (Liu and Nocedal, 1989) is then used to minimize the cost function iteratively, taking as input the cost function and its gradient. Such iterative optimizations using GEOS-Chem and its adjoint have been discussed in details previously (Henze et al., 2007, 2009; Kopacz et al., 2009, 2010).

3.2 Error specifications

A key aspect of inverse modeling is the specification of the error covariance matrices of variable parameters and obser-

vations (Palmer et al., 2003; Heald et al., 2004). We set the a priori and observation errors following Mao et al. (2014). We assume for separate inversions presented here an uncertainty of 30, 50, or 200 % for anthropogenic BC emissions and 300 or 500 % for biomass burning BC emissions. We assume that the a priori errors are spatially uncorrelated. The spatial correlations between the a priori errors have been proved to improve the inversion, particularly in regions adjacent to strong sources and less directly constrained (Stavrakou and Müller, 2006). For example, the assumption of no spatial correlation between a priori errors would underestimate the biomass burning emissions in regions close to the extensive agriculture fires. We set the observation error at 30, 50, or 100 %, which includes the model, representation, and measurement errors. Setting these errors in relative terms can become problematic when the observed BC concentrations are vanishingly small. These small values tend to skew the inversion toward matching the minimal errors. We thus set an absolute error of 0.04 µg m^{-3} based on the estimated observation errors. We showed previously that the combination of 50 % uncertainty for anthropogenic emissions, 500 % uncertainty for biomass burning emissions, and 30 % total observation error provided the best retrieval results in the analytical inversions (Mao et al., 2014). We adopt this set of error specifications in the standard inversion in the present study (Case 1, Table 1). The results are compared with those from the analytical inversions of Mao et al. (2014).

3.3 Emission scaling factors X/X_{a}

We optimize here the scaling factors of emissions X/X_{a} (rather than the actual emissions X), as a standard practice in adjoint inversion studies (Henze et al., 2009). The form of the scaling factors in an adjoint inversion is crucial for the inversion to efficiently and rapidly converge to a solution (Jiang et al., 2015b). When the optimization is directly on the scaling factors expressed linearly as X/X_{a} (i.e., the cost function gradient is computed with respect to X/X_{a}), the regions with strong a priori emissions tend to dominate the optimization, manifested in unrealistically large changes of emissions in these regions but limited variations in the regions with weak a priori emissions. Alternatively, when the optimization is instead on the logarithm of the scaling factors, $\ln(X/X_{\mathrm{a}})$ (i.e., the cost function gradient is now computed with respect to $\ln(X/X_{\mathrm{a}})$), the optimization can potentially result in an unbalanced convergence that is much faster for the regions with positive biases than for the regions with negative biases. Here we calculate cost function gradients with a hybrid form of scaling factors (Jiang et al., 2015b),

$$
\text{gradients} = \begin{cases} \dfrac{x}{x_{\mathrm{a}}} \leq 1 & \dfrac{\partial J}{\partial \ln(x/x_{\mathrm{a}})} = \dfrac{\partial J}{\partial x} \times x_{\mathrm{a}} \times \dfrac{x}{x_{\mathrm{a}}} \\ \dfrac{x}{x_{\mathrm{a}}} > 1 & \dfrac{\partial J}{\partial \frac{1}{2}\left[(x/x_{\mathrm{a}})^2 - 1\right]} = \dfrac{\partial J}{\partial x} \times x_{\mathrm{a}}/\dfrac{x}{x_{\mathrm{a}}} \end{cases}, \tag{4}
$$

so that the resulting optimization converges equally efficiently for the regions with positive or negative biases.

3.4 The regularization parameter γ_r

The assumption that a priori errors are spatially uncorrelated hinges on the consideration that the spatial resolution of the CTM is much larger than the correlation length scale of the individual emission sources (Henze et al., 2009). However, the uncertainties of emissions from different model grid boxes (e.g., $\sim 200 \times 250\,\mathrm{km}^2$ at $2° \times 2.5°$) within a region (e.g., a country) are usually correlated (Stavrakou and Müller, 2006). Without explicitly enforcing these correlations, a regularization parameter, which ensures a smooth solution to the inversion, is often used to rectify the aforementioned inconsistency, by ensuring the a posteriori emissions remain sufficiently close to the a priori values, which themselves reflect such correlations owing to the nature of bottom-up emissions inventories (Rodgers, 2000; Henze et al., 2009). Here we use the regularization parameter γ_r to balance the two terms of the cost function (Eq. 3) (Hakami et al., 2005; Müller and Stavrakou, 2005; Henze et al., 2007; Kopacz et al., 2009). A large γ_r relaxes the solution toward the a priori constraint while limiting the influence of the observation term, resulting in over-smoothing of the solution. In contrast, a small γ_r largely curtails the influence of the a priori constraint. To find an optimal γ_r value, we conduct inversions with a range of γ_r (10, 1, 0.1, 0.01, 0.001, and 0.0001). The resulting a posteriori cost function values, normalized by the initial value, are shown in Fig. S2 (top). We use $\gamma_r = 0.001$ in the analysis hereinafter, as that provides a small normalized a posteriori cost function and a sufficient cost function reduction.

As an example, Fig. S2 (bottom) shows the cost function reduction for August 2006. We regard the minimization as having converged sufficiently when the cost function changes less than 2 % during the last three iterations. The cost function converges in 10–20 iterations (35 % reduction at $2° \times 2.5°$ and 50 % at $0.5° \times 0.667°$). The cost function values are of the same order as the number of observations used in the inversion (~ 690). The penalty term (Sect. 3.1) is a mere 3 % of the a posteriori cost function at $2° \times 2.5°$ and 8 % at $0.5° \times 0.667°$; therefore the influence of the a priori is likely rather modest.

4 Results and discussion

Our standard adjoint inversion is at $2° \times 2.5°$, with uncertainties of 50 % for anthropogenic emissions, 500 % for biomass burning emissions, and 30 % for the observation (Case 1, Table 1). The a posteriori emissions are 49.9 Gg at $2° \times 2.5°$ and 47.3 Gg at $0.5° \times 0.667°$ for July–September, substantially higher than the a priori (24.3 Gg), because the modeled surface BC concentrations are largely biased low at most IMPROVE sites (Mao et al., 2011, 2014).

We focus our discussions hereinafter on August only, unless stated otherwise, for the sake of concision and clarity.

Figure 2 shows the a priori and the a posteriori monthly anthropogenic and biomass burning BC emissions from the standard adjoint inversion for August. The anthropogenic and biomass burning emissions are adjusted (higher or lower) alike in most grid boxes. Both the anthropogenic and biomass burning emissions increase 2-fold overall. The biomass burning emissions increase by varying factors (Table 1): 2.3 in the Rockies, 2.8 in California and the Southwest, and 1.5 in the Pacific Northwest; the regions are defined as in Mao et al. (2014).

The sensitivity of the cost function $J(X)$ to the BC emissions is a useful metric for evaluating the inversions. Following Henze et al. (2009), we normalize the sensitivity as follows:

$$\frac{\partial J(X)}{\partial x_{m,i}} \frac{x_{m,i}}{J(X)}. \tag{5}$$

It is the percentage of the cost function response to the fractional change in the BC emission source m (biomass burning, anthropogenic or total emissions) in model grid box i. As such, negative sensitivities are regions in which the model underestimates actual emissions and an increase of BC emissions would improve model agreement with the observations. It is the opposite for positive sensitivities. The results for August are shown in Fig. 3. The largest negative sensitivities to biomass burning emissions are in Washington, Ohio, Idaho, and California, where the model severely underestimates the biomass burning emissions and the sensitivities decrease significantly after the inversions. The inversions generally result in large reductions to both the positive and negative sensitivities ($\sim 90\,\%$ on average at $2° \times 2.5°$ and $0.5° \times 0.667°$).

4.1 Sensitivity analyses

Here we examine the sensitivity of the adjoint inversions to error specifications, choice of observations, collocated emissions, and the model resolution. These sensitivity analyses also provide a measure of the robustness of the inversions (Mao et al., 2014). For that purpose we conduct adjoint inversions at $2° \times 2.5°$ and $0.5° \times 0.667°$ (Cases 2–8, Table 1) in addition to the standard inversion (Case 1), with assorted a priori and observation errors, different subsets of the IMPROVE data, and collocated anthropogenic and biomass burning emissions. The results are compared and contrasted with those from the standard adjoint inversion in the discussions hereafter, unless stated otherwise. We find that the inversions generally show comparable and consistent results with those from the standard inversion. The ensemble a posteriori biomass burning emissions (Cases 1–8) are 4.6–6.5 Gg (a factor of 1.7–2.3 relative to the a priori) and anthropogenic emissions 8.6–12.8 Gg (a factor of 1.5–2.2 increase).
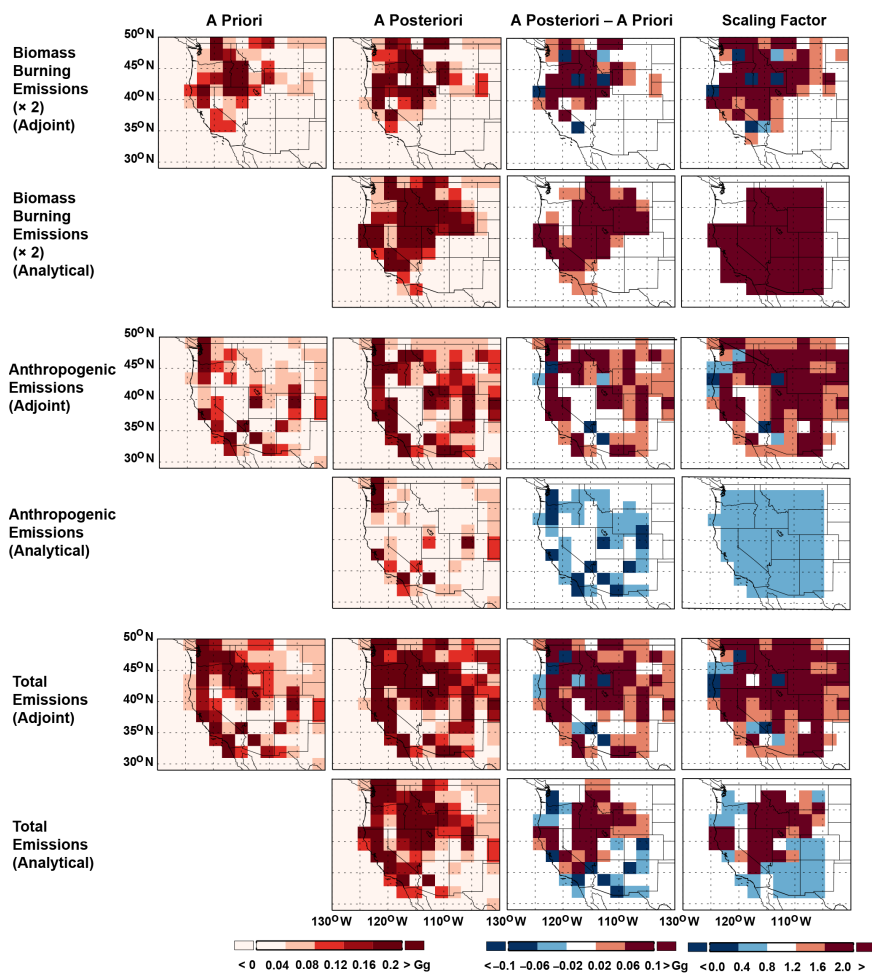
Figure 2. Emissions of BC in the WUS for August 2006: (top two rows) biomass burning, (middle two rows) anthropogenic, and (bottom two rows) total emissions. First column – the a priori; second column – the optimized inventory; third column – differences between the a posteriori and a priori; fourth column – scaling factors. For the purpose of clarity, biomass burning emissions are multiplied by 2 in the figures. Retrieval results are from the standard adjoint (Case 1, Table 1) and analytical (Mao et al., 2014) inversions at $2° \times 2.5°$. We assume for inversions uncertainties of 500, 50, and 30 % for biomass burning BC emissions, anthropogenic BC emissions, and total observation error.

4.1.1 Error specifications

We first conduct adjoint inversions (Cases 2–5) to examine the sensitivity of the inversions to the a priori and observation errors. The a posteriori emissions are 3 % lower when we reduce the uncertainty of the a priori biomass burning emissions from 500 to 300 % (Case 2). Reducing the uncertainty of the a priori anthropogenic emissions from 50 to 30 % brings no appreciable change to the a posteriori emissions (Case 3). Quadrupling that uncertainty (from 50 to 200 %) increases the a posteriori emissions by 10 % (Case 4). We find that the inversions are more sensitive to the observation error than the a priori error. For instance, an increase from 30 to 100 % of the observation error (Case 5) results in a 16 % decrease in the a posteriori emissions.

4.1.2 Choices of observations

A robust inversion critically relies on the spatiotemporal coverage of the observations. For carbon dioxide, a minimum of 10 sites per region were needed in analytical inversions (Gloor et al., 1999). For BC, the number of site is usually smaller. Only ~ 1000 BC observations were used to optimize $\sim 20\,000$ variables in an adjoint study (Hakami et al., 2005) during ACE-Asia (Huebert et al., 2003; Seinfeld et al., 2004). In this study, we use ~ 690 observations to constrain ~ 600 variables at $2° \times 2.5°$ and $\sim 10\,000$ at $0.5° \times 0.667°$.

Here we conduct two inversions to probe the sensitivity of the inversion to observations by using subsets of the IM-PROVE data and comparing the results with those from the standard inversion (Case 1). In the inversion (Case 6), we set aside 13 (~ 20 % of the 69) sites with $\chi^2 > 1.5$ and large
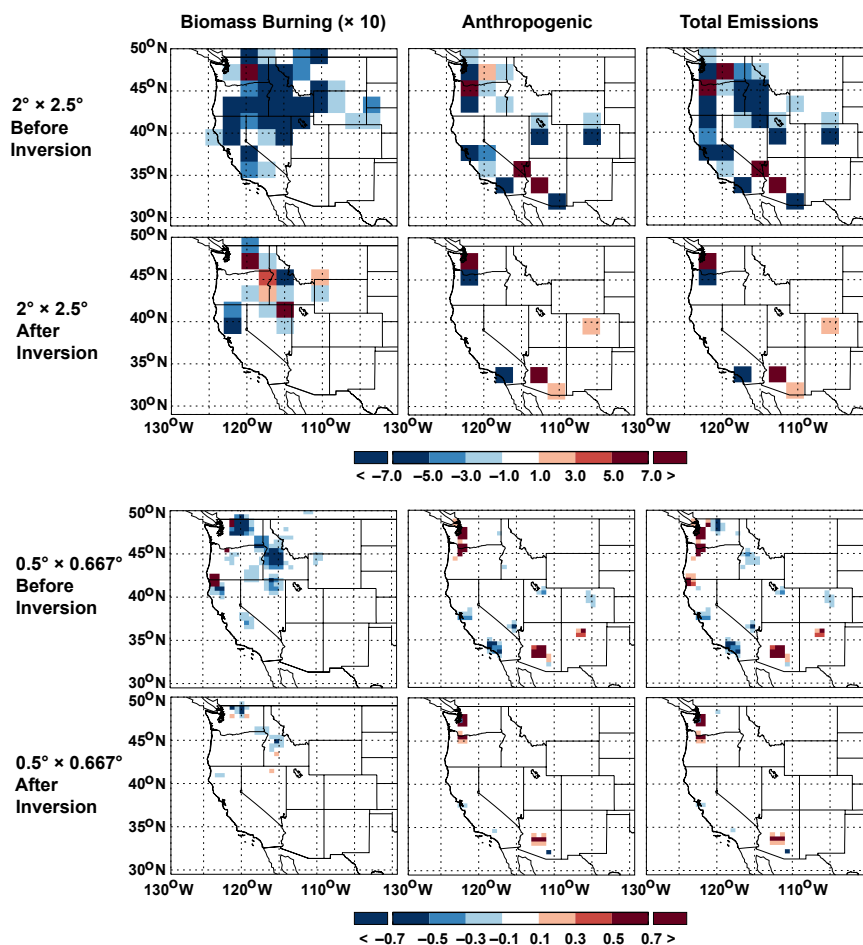
Figure 3. Normalized sensitivities of the cost function with respect to the BC emissions (left: biomass burning BC; middle: anthropogenic BC; right: total emissions of BC) before and after the inversions at $2° × 2.5°$ (Case 1, Table 1) and $0.5° × 0.667°$ (Case 9, same as Case 1, except at $0.5° × 0.667°$) for August 2006. For the purpose of clarity, sensitivities of the cost function to biomass burning emissions are multiplied by 10 in the figures.

model–observation departure ($> 0.5 \, \mu g \, m^{-3}$). χ^2 is calculated as the square of the ratio of the difference between modeled and observed surface BC concentrations to the observation accuracy. The measurements from these 13 sites are used as independent observations, whereas the measurements from the remaining 56 sites are used in the inversion. We find that the resulting a posteriori emissions (Fig. 4) are within 6 % of those from Case 1 (Fig. 2). The emissions differ significantly only in ∼ 10 % of the grid boxes, mainly in the Pacific Northwest and the Rockies. The resulting surface BC concentrations averaged over the 13 sites are within 15 % between the two cases. There is a ∼ 15 % reduction in the mean bias of the surface BC concentrations (averaged over the 13 sites) for Case 6 and 20 % for Case 1. In another inversion (not shown), we set aside 4 (∼ 5 % of the 69) sites with $\chi^2 > 2$. The results are also consistent with those from Case 1.

4.1.3 Collocated emissions

In the WUS mountain ranges, biomass burning BC emissions are substantially underestimated (Mao et al., 2011). There are large uncertainties in the temporal variation and spatial distribution of fire emissions (Langmann et al., 2009). Small fires are likely a major source of these uncertainties (Randerson et al., 2012). For instance, small fires can lead to large relative errors (50–100 %) in burned area estimates (Korontzi et al., 2006; Giglio et al., 2006, 2010; McCarty et al., 2009; Roy and Boschetti, 2009).

Figure 5 shows monthly anthropogenic and biomass burning emissions in each $2° × 2.5°$ model grid box in the WUS. Collocated anthropogenic and biomass burning emissions are in most of the grid boxes. The anthropogenic emissions are larger than the biomass burning emissions in 80 % of the grid boxes and still significant in the remaining 20 %. Here we conduct two inversions (Cases 7–8) to examine the ability of the adjoint inversion system to distinguish collocated
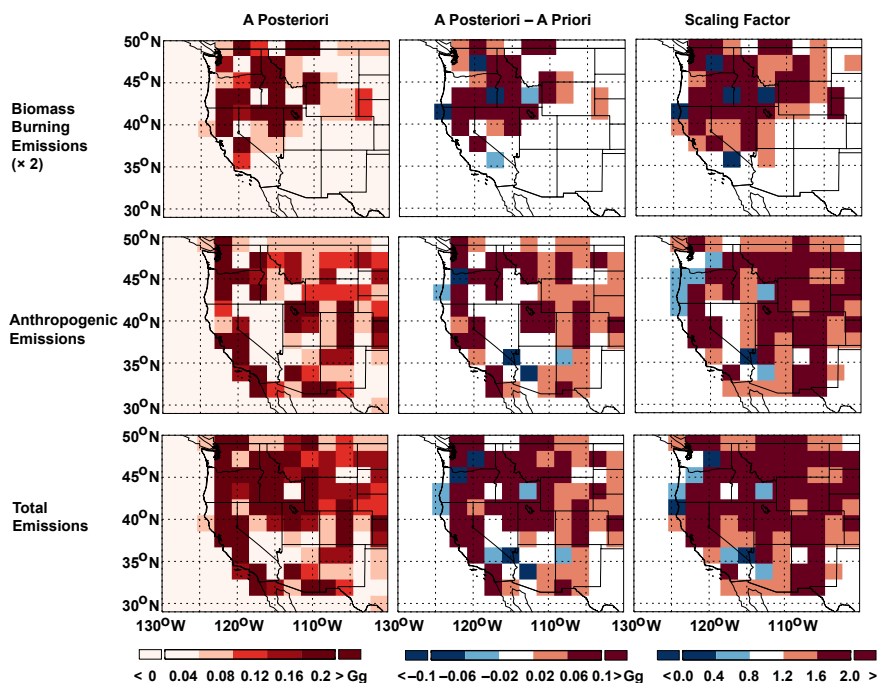
Figure 4. Emissions of BC in the WUS for August 2006: (top panels) biomass burning, (middle panels) anthropogenic, and (bottom panels) total emissions. Results are from Case 6 (Table 1): (left column) the optimized inventory, (middle column) a posteriori–a priori, and (right column) the scaling factors. Case 6 is same as Case 1, except with only 56 sites used in the inversion. For the purpose of clarity, biomass burning emissions are multiplied by 2 in the figures.
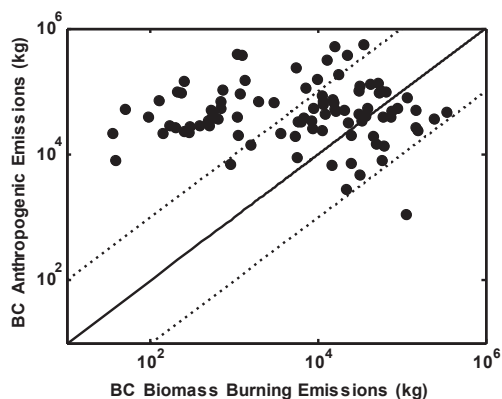

Figure 5. Monthly anthropogenic and biomass burning emissions of BC in each $2° × 2.5°$ grid box for August 2006 (unit: kg). Solid line is 1:1 and dashed lines are 1 : 10 (or 10 : 1).

biomass burning versus anthropogenic emissions, especially in the regions where the biomass burning emissions are likely underestimated. We conduct one inversion (Case 7) on the total emissions, considering an error of 200 % for the a priori emissions. We find that the resulting total a posteriori emissions increase by a factor of 2.2 relative to the a priori and are within 2 % of those from Case 1. We conduct another inversion (Case 8) to examine how much the inversion can distinguish the collocated emissions. In each grid box, we

add 2.5 Mg (∼ 10 % of the maximum emissions among the grid boxes) as a diagnosis to the (a priori) biomass burning emissions of BC and examine the degree to which the inversion results change the partitioning of biomass burning versus anthropogenic emissions by comparing the inversion results with those from Case 1 (or Case 7). The differences in the a posteriori emissions of BC between Cases 8 and 1 are shown in Fig. 6. The anthropogenic and biomass burning emissions from Case 8 show opposite and disproportional changes, relative to the corresponding emissions from Case 1. Specifically, there is an approximately linear increase (i.e., Case 8 relative to Case 1) in the biomass burning emissions (by more than 5 Mg in nearly every grid box) and a linear decrease (again, Case 8 relative to Case 1) in the anthropogenic emissions (by ∼ 3 Mg, except in California). However, the anthropogenic and biomass burning emissions of BC, when summed over the WUS, each increase 2-fold (relative to the corresponding a priori) in both Case 8 and Case 1; the total emissions remain essentially the same (less than 1 % difference) between the two cases (Table 1). The inversion system tends to overcompensate the deficit of biomass burning emissions by disproportionately increasing anthropogenic emissions instead in the same grid box. This indicates that the inversion system lacks the ability to effectively distinguish collocated biomass burning and anthropogenic emissions in the WUS on model grid scales.
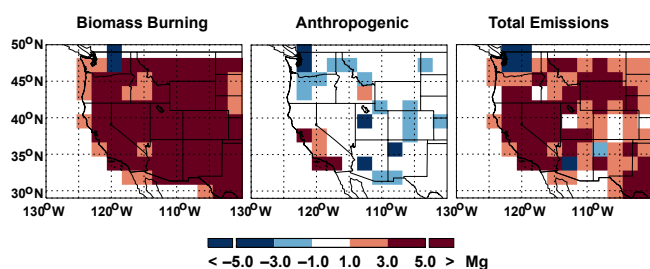
Figure 6. Emissions of BC: Case 8 minus Case 1 (Table 1) at $2° \times 2.5°$ for August 2006. Case 8 is same as Case 1, except with the a priori biomass burning emissions uniformly increased by 2.5 Mg in every model grid box.

4.1.4 Model resolution

GEOS-Chem simulations generally provide better agreements with observations at $0.5° \times 0.667°$ than at $2° \times 2.5°$ for CO (Wang et al., 2004; Chen et al., 2009), ozone (Zhang et al., 2011), mercury (Zhang et al., 2012), and BC (Mao et al., 2014). We found in a companion study (Mao et al., 2014) that the a posteriori BC emissions from analytical inversions of the IMPROVE observations were considerably lower at $0.5° \times 0.667°$ than at $2° \times 2.5°$. Intuitively, the larger smearing of the emissions at the coarser resolution results in larger model–observation discrepancies (Chen et al., 2009). The larger discrepancies in turn tend to drive the inversion system toward imposing larger emissions at the coarser than the finer resolutions when minimizing the said discrepancies.

As a comparison to the standard inversion at $2° \times 2.5°$ (Case 1), we conduct another adjoint inversion at $0.5° \times 0.667°$ (Case 9) with the same error specifications. The resulting a posteriori emissions are shown in Fig. 7. The biomass burning emissions are 53 % larger in Case 9 than in Case 1 in the Pacific Northwest but 27 % lower in the Rockies and 43 % lower in California and the Southwest. The total emissions are considerably lower at $0.5° \times 0.667°$ (27 % lower for anthropogenic and 10 % for biomass burning) yet provide better agreement with the observations (Sect. 4.4). The a posteriori emissions from the standard analytical inversion (Mao et al., 2014) are also shown in Fig. 7 for comparison. The differences between the analytical and adjoint inversions (Table 1) are slightly larger at $0.5° \times 0.667°$ (53 %) than at $2° \times 2.5°$ (39 %). The larger differences reflect in part that the adjoint inversion system has even more difficulty in constraining the emissions at the finer grid scale (Sects. 4.1.3 and 4.2).

4.2 Pseudo observations

We use pseudo observations of BC concentrations in another group of inversions (Table 2) to further examine the sensitivity of the adjoint inversions to collocated emissions, error specifications, and observations. We generate the pseudo ob-

servations by increasing the a priori biomass burning emissions of BC in each grid box 3-fold. The total amount of the a priori emissions added is 5.6 Gg. The frequency of the pseudo observations are 24 h averages for every 3 days, following the IMPROVE measurements of BC. We then invert the pseudo observations at $2° \times 2.5°$ and with the same a priori emissions as those used in the standard inversion (Case 1). We examine whether the inversions are able to fully recover the emissions used to generate the pseudo observations. Specifically, we expect the a posteriori biomass burning emissions to increase 3-fold relative to the a priori, whereas the anthropogenic emissions remain unchanged.

We first conduct two inversions (Pseudos 1–2) to investigate the ability of the adjoint inversion system to distinguish collocated anthropogenic and biomass burning emissions. We consider two extreme scenarios: the pseudo observations are in every surface grid box (Pseudo 1) and in every grid box in the lowest 15 vertical layers (Pseudo 2). Other aspects of the two inversions remain the same as those of the standard inversion (Case 1). We find that the results are nearly indistinguishable. The a posteriori cost function is greatly reduced (by 95 % in Pseudo 1 and by 97 % in Pseudo 2). The a posteriori emissions both increase by exactly 5.6 Gg, fully recovering the added biomass burning emissions. However, the increase is uneven and not limited to the biomass burning emissions. The biomass burning emissions increase by a factor of 2.3 and anthropogenic emissions by a factor of 1.3. The inversions thus falsely impose larger anthropogenic emissions to minimize the large discrepancies between the model predictions and the pseudo observations.

In the next three inversions (Pseudos 3–5), we examine the sensitivity of the inversion system to the constraints for anthropogenic versus biomass burning emissions. The uncertainty of the anthropogenic emissions is reduced to 10 % in Pseudo 3. We assume that the anthropogenic emissions are perfect and leave them unchanged in Pseudo 4. In Pseudo 5, we let the biomass burning emissions remain unaltered. Other aspects of Pseudos 3–5 remain the same as those of Pseudo 1. We find that the resulting a posteriori emissions from the former two (Pseudos 3 and 4) recover fully the added (biomass burning) emissions. The biomass burning emissions increase by a factor of 2.5 in Pseudo 3 (versus 2.3 in Pseudo 1) and by a factor of 2.9 in Pseudo 4. However, the a posteriori emissions from Pseudo 5 increase by only 4.2 Gg, recovering just 75 % of the added (biomass burning) emissions.

Concurrent measurements of other combustion tracers, for example, CO and carbon isotopes, can conceivably provide additional information to distinguish collocated BC emissions. Previous studies have shown that the ratio of BC to CO significantly varies with the fuel types and thus is a good indicator for identifying BC sources (Spackman et al., 2008; Han et al., 2009; Subramanian et al., 2010; Reche et al., 2011). Carbon isotopes such as ^{14}C are known to be present at small and more or less constant levels in biogenic emissions but
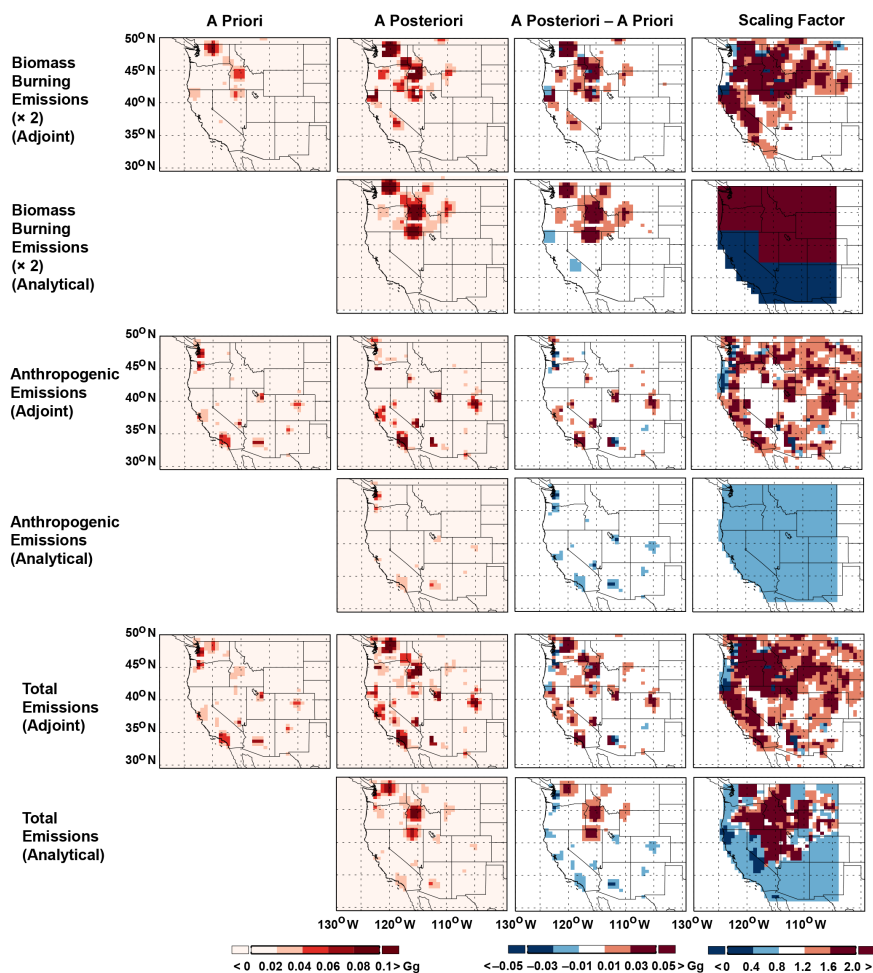
Figure 7. Same as Fig. 2, but at $0.5° \times 0.667°$ (Case 9, same as Case 1, except at $0.5° \times 0.667°$).

absent in fossil fuels (Schichtel et al., 2008). Ample studies heretofore have shown that ^{14}C is useful for analyzing the source apportionment of atmospheric carbonaceous aerosols (Heal, 2014, and references therein). [14]C measurements are currently only available from short-term studies in part because of the relatively high cost of deploying such measurements in routine monitoring networks (Lewis et al., 2004; Bench et al., 2007; Bench, 2004; Szidat et al., 2006).

Additionally, we conduct four inversions (Pseudos 6–9) to examine the minimum number of observation sites needed for the inversions. The inversions are the same as Pseudo 1, except that the pseudo observations are randomly distributed in 75 % (Pseudo 6), 50 % (Pseudo 7), or 25 % (Pseudo 8) of the surface grid boxes, or in the surface grid boxes with larger than five fire counts per month (covering ~ 50 % of surface grid boxes, Pseudo 9). The resulting a posteriori emissions recover 94 % (Pseudo 6), 93 % (Pseudo 7), 80 % (Pseudo 8), and 93 % (Pseudo 9) of the added (biomass burning) emissions. Randomly, surface observations covering at least 50 % of the model grid boxes are needed to estimate the total BC emissions on the model grid scale. In our case, 69 IMPROVE

sites are used to constrain BC emissions in ~ 100 surface grid boxes at $2° \times 2.5°$ and ~ 1500 at $0.5° \times 0.667°$. As we discussed in Sect. 4.1.2, the differences between the inversion results with 69 or 56 IMPROVE sites are essentially small, indicating that the 69 or 56 sites alone (excluding other observations) are likely sufficient only for constraining the total emissions of BC, especially at $2° \times 2.5°$. With pseudo observations located at biomass burning source regions (Pseudo 9), the resulting a posteriori biomass burning emissions are 5 % higher than those from the inversion with similar amount of pseudo observations (in 50 % of surface grid boxes, Pseudo 7), whereas the total a posteriori emissions are almost unchanged between Pseudos 7 and 9. Thus, pseudo observations located at source regions would be more effective to constrain sources.

4.3 Adjoint versus analytical inversions

The analytical method is limited to constraining emissions over aggregated regions because of computational limitations, whereas the adjoint method is able to describe emission

Table 2. Monthly anthropogenic and biomass burning emissions of BC (unit: Gg) in the WUS from the adjoint inversions for August 2006 using pseudo observations.

		Inversion configurations			Emissions (Gg (10^9 g))			$J(x)$ reduction[c]
		Pseudo observations	S_aANTH (%)	S_aBB (%)	Anth.	BB	Δ Emissions[b]	(%)
A posteriori	Pseudo 1	every surface grid box	50	500	7.7 (1.3[a])	6.5 (2.3)	5.6 (2.0)	95
	Pseudo 2	every grid box in the lowest 15 layers	50	500	7.8 (1.3)	6.4 (2.3)	5.6 (2.0)	97
	Pseudo 3	every surface grid box	10	500	7.1 (1.2)	6.9 (2.5)	5.4 (1.9)	95
	Pseudo 4	every surface grid box	0	500	5.8 (1.0)	8.2 (2.9)	5.4 (1.9)	99
	Pseudo 5	every surface grid box	50	0	10.0 (1.7)	2.8 (1.0)	4.2 (1.5)	55
	Pseudo 6	randomly in 75 % of the surface grid boxes	50	500	7.8 (1.3)	6.2 (2.2)	5.4 (1.9)	94
	Pseudo 7	randomly in 50 % of the surface grid boxes	50	500	8.0 (1.4)	5.9 (2.1)	5.3 (1.9)	93
	Pseudo 8	randomly in 25 % of the surface grid boxes	50	500	7.5 (1.3)	5.3 (1.9)	4.2 (1.5)	96
	Pseudo 9	in the surface grid boxes with fire counts (> 5)	50	500	7.6 (1.3)	6.2 (2.2)	5.2 (1.9)	95
"Ghost" emissions[d]					5.8 (1.0)	8.4 (3.0)	5.6 (2.0)	
A priori					5.8	2.8		

[a] Scaling factors in parentheses. [b] The increase of total emissions relative to the a priori biomass burning emissions (ratio of the total emissions change over the a priori biomass burning emissions in parentheses). [c] The reduction of the a posteriori cost function relative to the a priori. [d] Emissions (with anthropogenic emissions unchanged but biomass burning emissions tripled) used to generate the pseudo observations for Pseudos 1–9.
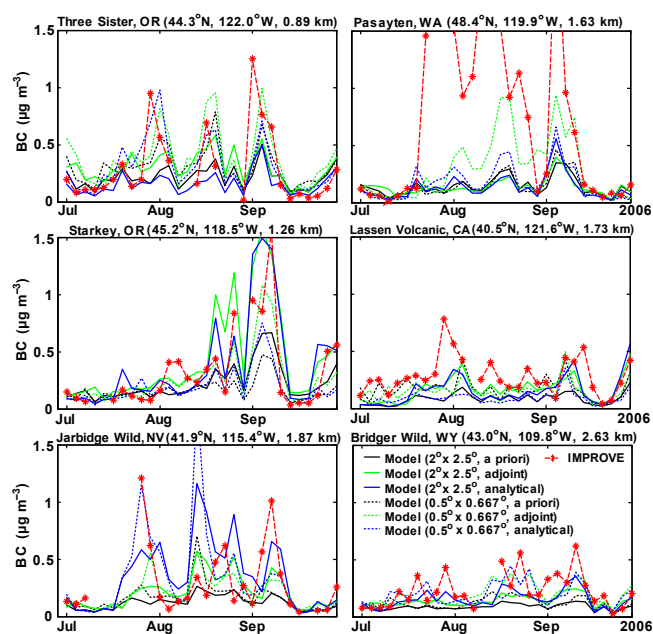

Figure 8. Observed (red line) and GEOS-Chem simulated 24 h average surface BC concentrations ($\mu g\,m^{-3}$) at six IMPROVE sites for July–September 2006. Results are for $2° \times 2.5°$ (solid) and $0.5° \times 0.667°$ (dotted line) with the a priori (black line) or a posteriori emissions from the analytical (blue line) or adjoint (green line) inversions.

variability on finer scales and more efficiently (Kopacz et al., 2009). There are large differences in the a posteriori emissions between the analytical and adjoint inversions, not only in the spatial distributions but also in the magnitudes (Figs. 5 and 10). In California, for example, the a posteriori biomass burning emissions at $0.5° \times 0.667°$ increase in the adjoint inversion but decrease in the analytical inversion, relative to the a priori. In the WUS, the analytical inversions show a factor of 3–5 increase of the biomass burning emissions and a $\sim 50\%$ reduction of the anthropogenic emissions, relative to the corresponding a priori (Mao et al., 2014). In contrast, both the biomass burning and anthropogenic emissions in the adjoint inversions increase 2-fold (Table 1). The total a posteriori emissions are rather comparable (within 20–50 %) between the two inversions.

Mao et al. (2014) have examined in detail the quality of the analytical inversions. The robustness of the analytical inversions and the relative consistency in the total a posteriori emissions from the two inversion methods therefore imply that the adjoint inversion results, at least the total emissions, are robust on the model grid scale. We will examine the robustness of the adjoint inversions further in Sect. 4.4. The large differences in the a posteriori anthropogenic and biomass burning emissions between the two inversion methods are largely because the inversion system has difficulty effectively distinguishing collocated biomass burning and anthropogenic emissions on model grid scales. As a result, the adjoint inversions tend to falsely impose larger anthropogenic emissions in the regions where the collocated biomass burning emissions are too low (Sects. 4.1.3 and 4.2). Jiang et al. (2011) also found that the adjoint inversion system is unable to distinguish CO emissions from collocated combustion and oxidation sources and they therefore lumped the two sectors in their inversions. The differences are also
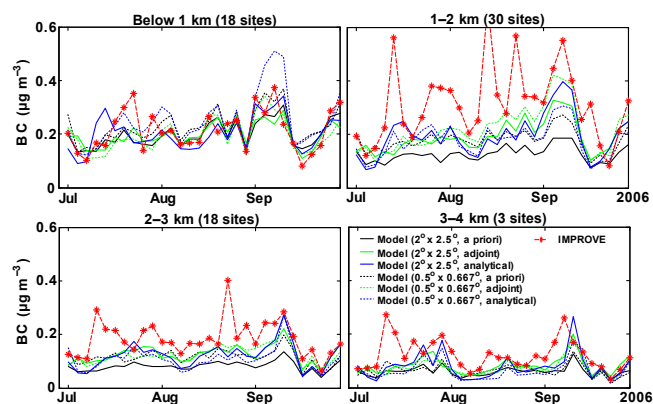
Figure 9. Observed (red line) and GEOS-Chem simulated 24 h average surface BC concentrations ($\mu g\,m^{-3}$) for July–September 2006, averaged for the IMPROVE sites (Fig. 1) in altitudes below 1 km (18 sites), 1–2 km (30 sites), 2–3 km (18 sites), and above 3 km (3 sites). Results are for $2° \times 2.5°$ (solid line) and $0.5° \times 0.667°$ (dotted line) with the a priori (black line) or a posteriori emissions from the analytical (blue line) or adjoint (green line) inversions.

Figure 10. Differences between GEOS-Chem simulated and observed 24-hour average surface BC concentrations at the 69 IMPROVE sites (Fig. 1) for August 2006. Model results are from the adjoint inversions at $2° \times 2.5°$ (Case 1, Table 1) and $0.5° \times 0.667°$ (Case 9, same as Case 1, except at $0.5° \times 0.667°$) with the a priori or a posteriori emissions.

due to the large aggregation errors in the analytical inversions and the assumption of spatially uncorrelated a priori errors in the adjoint inversions (Sects. 3.2 and 3.4).

We further separate the anthropogenic-dominated regions to examine the ability of the adjoint inversion system to constrain collocated emissions. In the regions where anthropogenic emissions are dominant, model surface BC concentrations are in good agreement with IMPROVE observations (Mao et al., 2011) and both the a posteriori anthropogenic and biomass burning emissions see substantial yet still relatively small increases. For example, the a posteriori anthropogenic and biomass burning emissions in Washington and Oregon increase by 39 and 29 %. However, in the regions where biomass burning emissions become more important but significantly underestimated, model surface BC concentrations are biased low and both the a posteriori anthropogenic and biomass burning emissions increase dramatically. For example, in Montana, Idaho, and Wyoming, the a posteriori anthropogenic and biomass burning emissions increase by factors of 2.2 and of 2.7. In Utah, Colorado, Arizona, and New Mexico, the corresponding emissions increase by factors of 1.8 and of 1.3. In California and Nevada, the emissions increase both by a factor of 1.8.

4.4 Evaluation against observations

Model simulated surface BC concentrations with the a posteriori emissions show significant enhancements and largely reproduce both the synoptic variability and magnitudes of the observed surface BC concentrations, not only at individual sites (Fig. 8) but also on average at four altitude ranges (below 1, 1–2, 2–3, and above 3 km) (Fig. 9). For instance, model surface BC concentrations after the adjoint inversions
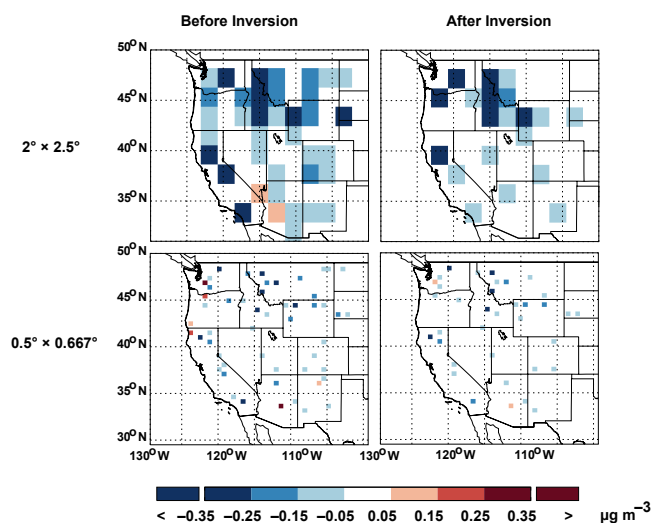
capture the major fire episodes at Starkey, OR (45.2° N, 118.5° W, 1.26 km) and Lassen Volcanic, CA (40.5° N, 121.6° W, 1.73 km). The adjoint inversions at $0.5° \times 0.667°$ provide better agreements with the observations than the analytical inversion results do at some sites, for example, Three Sisters, OR (44.3° N, 122.0° W, 0.89 km) and Pasayten, WA (48.4° N, 119.9° W, 1.63 km). At other sites, Jarbidge Wild, NV (41.9° N, 115.4° W, 1.87 km), for example, results from the analytical inversions are noticeably better. The two inversion results differ the most at 1–2 km altitudes and to a lesser degree at higher altitudes, for example, Bridger Wild, WY (43.0° N, 109.8° W, 2.63 km). The a posteriori emissions lead to an average bias reduction of ∼ 50 % in the simulated surface BC concentrations at 1–2 km altitudes (Fig. 9). Model simulated surface BC concentrations with the a posteriori emissions from the adjoint inversions, especially at $0.5° \times 0.667°$, show substantial enhancements during major fire episodes. The enhancements are evident at all altitudes (up to 0.2 $\mu g\,m^{-3}$ at 1–2 km and 0.1 $\mu g\,m^{-3}$ at 2–3 km). The a posteriori emissions lead to large mean bias reductions (34 % at $2° \times 2.5°$ and 20 % at $0.5° \times 0.667°$ for August), as shown in Fig. 10. The frequency distributions of the bias of the 24 h average surface BC concentrations are Gaussian (Fig. 11), as expected. The inversions reduce both the mean (by ∼ 35 % at $2° \times 2.5°$ and ∼ 15 % at $0.5° \times 0.667°$ for July–September) and standard deviation of the biases.

Taylor diagram and skill score (S) are useful measures of model accuracy. The diagram relates the centered root mean square error (RMSE), the pattern correlation (r) and the standard deviation (σ) of observations and model results (Taylor,
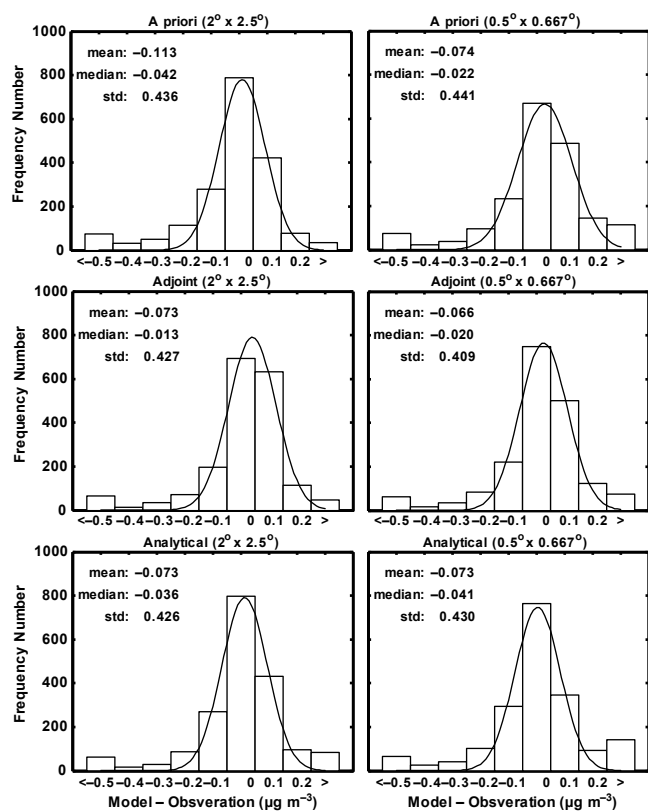
Figure 11. Frequency distribution of the bias of GEOS-Chem simulated 24 h average surface BC concentrations for July–September 2006. Results are for $2° \times 2.5°$ and $0.5° \times 0.667°$ with the a priori or a posteriori emissions from the analytical or adjoint inversions. Also shown are the mean, median, standard deviation, and fitted Gaussian distribution.

Figure 12. Taylor diagram and Taylor scores for GEOS-Chem simulations of BC for July–September 2006 at $2° \times 2.5°$ (solid circle) and $0.5° \times 0.667°$ (open circle) with the a priori (red circle) or a posteriori emissions from the analytical (blue circle) or adjoint (green circle) inversions. Values are averages for the 69 IMPROVE sites (Fig. 1).

total emissions of BC, especially at the coarse resolution $2° \times 2.5°$. The inversion system however has difficulty in partitioning collocated anthropogenic versus biomass burning emissions. Furthermore, comparing localized observations with coarse-resolution model results is inherently problematic (Mao et al., 2011; Fairlie et al., 2007). It is even more so because many of the IMPROVE sites are mountainous and the associated upslope flow is difficult to represent in a global model.

5 Summary and conclusions

We have applied adjoint inversions to estimate biomass burning and anthropogenic emissions of BC in the WUS for July–September 2006 by inverting the surface BC concentrations from the IMPROVE network using the GEOS-Chem chemical transport model and its adjoint. The a posteriori emissions of BC differed considerably between the adjoint and analytical inversions (Mao et al., 2014), especially in the partitioning of anthropogenic versus biomass burning emissions. The total was ~20–50 % larger in the adjoint inversions than in the analytical inversions. Both the biomass burning and anthropogenic emissions from the adjoint inversions doubled, whereas the analytical inversions showed a factor of 3–5 increase in the former and a ~50 % reduction in the latter. We attributed these differences to the inability of the adjoint inversion system to effectively distinguish collocated biomass burning and anthropogenic emissions on the model grid scales. That inability resulted in excessively large anthropogenic emissions in the regions where biomass burning emissions were underestimated.

2001). S (0–1) increases with increasing correlations and as the modeled variance approaches the observed variance. Figure 12 presents the resulting diagram and skill scores of the observations and the multitude of model results. Model results with the a posteriori emissions are consistently in better agreement with the observations, especially using the nested model. The a posteriori emissions lead to higher r (by 11–48 % on average), larger σ (by 27–122 % on average), and lower centered RMSEs, thereby increasing the skill scores (by 43–221 %). The a posteriori emissions from the adjoint inversion at $0.5° \times 0.667°$ show the smallest centered RMSE and largest r, whereas the a posteriori emissions from the analytical inversion at $0.5° \times 0.667°$ show the largest σ and S values.

There are large uncertainties in the a posteriori emissions, as evident in the 20–30 % low bias in modeled surface BC concentrations. The uncertainties are partially because of the limitations of the inversion system, in both the nature of the inverse modeling and the spatiotemporal coverage of IMPROVE observations (see Sects. 4.1.3 and 4.2). The adjoint inversion system has sufficient information to constrain the
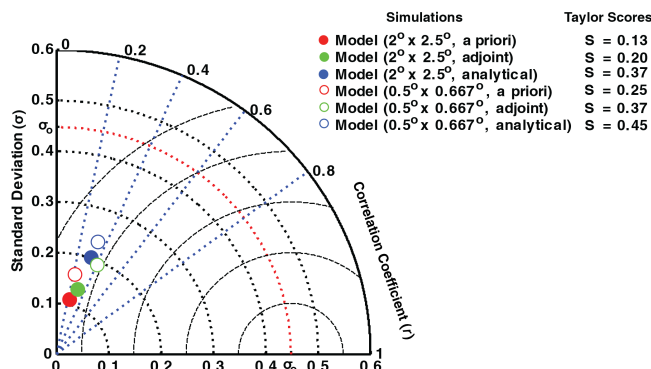
The inversions with various pseudo observations indicated that observations of surface BC concentration covering half of the model grid boxes had sufficient information to constrain the total emissions of BC on the model grid scales. IMPROVE observations of BC have sufficient information to constrain the total BC emissions at the model grid scales, especially at $2° \times 2.5°$. The limitations of the adjoint inversion system, including the spatiotemporal coverage of the IMPROVE observations of BC, call for concurrent measurements of other combustion tracers (e.g., CO and carbon isotopes). Other factors may also improve the inversions, e.g., increase measurements in the source regions, and considering the spatial correlation of the a priori errors in the inversions.

The Supplement related to this article is available online at doi:10.5194/acp-15-7685-2015-supplement.

References

Anenberg, S. C., Talgo, K., Arunachalam, S., Dolwick, P., Jang, C., and West, J. J.: Impacts of global, regional, and sectoral black carbon emission reductions on surface air quality and human mortality, Atmos. Chem. Phys., 11, 7253–7267, doi:10.5194/acp-11-7253-2011, 2011.

Anenberg, S. C., Schwartz, J., Shindell, D., Amann, M., Faluvegi, G., Klimont, Z., Janssens-Maenhout, G., Pozzoli, L., Van Dingenen, R., Vignati, E., Emberson, L., Muller, N. Z., West, J. J., Williams, M., Demkine, V., Hicks, W. K., Kuylenstierna, J., Raes, F., and Ramanathan, V.: Global air quality and health co-benefits of mitigating near-term climate change through methane and black carbon emission controls, Environ. Health Perspect., 120, 831–839, 2012.

Arellano, A. F., Kasibhatla, P. S., Giglio, L., van der Werf, G. R., and Randerson, J. T.: Top-down estimates of global CO sources using MOPITT Measurements, Geophys. Res. Lett., 31, L01104, doi:10.1029/2003GL018609, 2004.

Arellano, A. F., Kasibhatla, P. S., Giglio, L., van der Werf, G. R., Randerson, J. T., and Collatz, G. J.: Time-dependent inversion estimates of global biomass-burning CO emissions using Measurement of Pollution in the Troposphere (MOPITT) measurements,

J. Geophys. Res., 111, D09303, doi:10.1029/2005JD006613, 2006.

Arellano, A. F., Raeder, K., Anderson, J. L., Hess, P. G., Emmons, L. K., Edwards, D. P., Pfister, G. G., Campos, T. L., and Sachse, G. W.: Evaluating model performance of an ensemble-based chemical data assimilation system during INTEX-B field mission, Atmos. Chem. Phys., 7, 5695–5710, doi:10.5194/acp-7-5695-2007, 2007.

Bench, G.: Measurement of contemporary and fossil carbon contents of $PM_{2.5}$ aerosols: results from Turtleback Dome, Yosemite National Park, Environ. Sci. Technol., 38, 2424–2427, 2004.

Bench, G., Fallon, S., Schichtel, B., Malm, and W., McDade, C.: Relative contributions of fossil and contemporary carbon sources to $PM_{2.5}$ aerosols at nine Interagency Monitoring for Protection of Visual Environments (IMPROVE) network sites, J. Geophys. Res., 112, D10205, doi:10.1029/2006JD007708, 2007.

Bey, I., Jacob, D. J., Yantosca, R. M., Logan, J. A., Field, B. D., Fiore, A. M., Li, Q., Liu, H.-Y., Mickley, L. J., and Schultz, M. G.: Global modeling of tropospheric chemistry with assimilated meteorology: Model description and evaluation, J. Geophys. Res., 106, 23073–23095, 2001.

Bond, T. C., Streets, D. G., Yarber, K. F., Nelson, S. M., Woo, J.-H., and Klimont, Z.: A technology-based global inventory of black and organic carbon emissions from combustion, J. Geophys. Res., 109, D14203, doi:10.1029/2003JD003697, 2004.

Bond, T. C., Bhardwaj, E., Dong, R., Jogani, R., Jung, S., Roden, C., Streets, D. G., and Trautmann, N. M.: Historical emissions of black and organic carbon aerosol from energy-related combustion, 1850–2000, Global Biogeochem. Cy., 21, GB2018, doi:10.1029/2006GB002840, 2007.

Bond, T. C., Doherty, S. J., Fahey, D. W., Forster, P. M., Berntsen, T., DeAngelo, B. J., Flanner, M. G., Ghan, S., Kärcher, B., Koch, D., Kinne, S., Kondo, Y., Quinn, P. K., Sarofim, M. C., Schultz, M. G., Schulz, M., Venkataraman, C., Zhang, H., Zhang, S., Bellouin, N., Guttikunda, S. K., Hopke, P. K., Jacobson, M. Z., Kaiser, J. W., Klimont, Z., Lohmann, U., Schwarz, J. P., Shindell, D., Storelvmo, T., Warren, S. G., and Zender, C. S.: Bounding the role of black carbon in the climate system: A scientific assessment, J. Geophys. Res., 118, 5380–5552, doi:10.1002/jgrd.50171, 2013.

Cannon, S. H. and DeGraff, J.: The Increasing Wildfire and Post-Fire Debris-Flow Threat in Western USA, and Implications for Consequences of Climate Change, Springer, Verlag Berlin Heidelberg, 177–190, 2009.

Chai, T., Carmichael, G. R., Tang, Y., Sandu, A., Heckel, A., Richter, A., and Burrows, J. P.: Regional NOx emission inversion through a four-dimensional variational approach using SCIAMACHY tropospheric NO_2 column observations, Atmos. Environ., 43, 5046–5055, 2009.

Chen, D., Wang, Y., McElroy, M. B., He, K., Yantosca, R. M., and Le Sager, P.: Regional CO pollution and export in China simulated by the high-resolution nested-grid GEOS-Chem model, Atmos. Chem. Phys., 9, 3825–3839, doi:10.5194/acp-9-3825-2009, 2009.

Chevallier, F., Brèon, F.-M., and Rayner, P. J.: Contribution of the Orbiting Carbon Observatory to the estimation of CO_2 sources and sinks: Theoretical study in a variational data assimilation framework, J. Geophys. Res., 112, D09307, doi:10.1029/2006JD007375, 2007.

Chevallier, F., Fortems, A., Bousquet, P., Pison, I., Szopa, S., Devaux, M., and Hauglustaine, D. A.: African CO emissions between years 2000 and 2006 as estimated from MOPITT observations, Biogeosciences, 6, 103–111, doi:10.5194/bg-6-103-2009, 2009.

Fairlie, T. D., Jacob, D. J., and Park, R. J.: The impact of transpacific transport of mineral dust in the United States, Atmos. Environ., 41, 1251–1266, 2007.

Flanner, M. G., Zender, C. S., Randerson, J. T., and Rasch, P. J.: Present-day climate forcing and response from black carbon in snow, J. Geophys. Res., 112, D11202, doi:10.1029/2006JD008003, 2007.

Flanner, M. G., Zender, C. S., Hess, P. G., Mahowald, N. M., Painter, T. H., Ramanathan, V., and Rasch, P. J.: Springtime warming and reduced snow cover from carbonaceous particles, Atmos. Chem. Phys., 9, 2481–2497, doi:10.5194/acp-9-2481-2009, 2009.

Fu, T.-M., Cao, J. J., Zhang, X. Y., Lee, S. C., Zhang, Q., Han, Y. M., Qu, W. J., Han, Z., Zhang, R., Wang, Y. X., Chen, D., and Henze, D. K.: Carbonaceous aerosols in China: top-down constraints on primary sources and estimation of secondary contribution, Atmos. Chem. Phys., 12, 2725–2746, doi:10.5194/acp-12-2725-2012, 2012.

Giglio, L., van der Werf, G. R., Randerson, J. T., Collatz, G. J., and Kasibhatla, P.: Global estimation of burned area using MODIS active fire observations, Atmos. Chem. Phys., 6, 957–974, doi:10.5194/acp-6-957-2006, 2006.

Giglio, L., Randerson, J. T., van der Werf, G. R., Kasibhatla, P. S., Collatz, G. J., Morton, D. C., and DeFries, R. S.: Assessing variability and long-term trends in burned area by merging multiple satellite fire products, Biogeosciences, 7, 1171–1186, doi:10.5194/bg-7-1171-2010, 2010.

Gloor, M., Fan, S.-M., Pacala, S. W., Sarmiento, J. L., and Ramonet, M.: A model-based evaluation of inversions of atmospheric transport, using annual mean mixing ratios, as a tool to monitor fluxes of nonreactive trace substances like CO_2 on a continental scale, J. Geophys. Res., 104, 14245–14260, 1999.

Hakami, A., Henze, D. K., Seinfeld, J. H., Chai, T., Tang, Y., Carmichael, G. R., and Sandu, A.: Adjoint inverse modeling of black carbon during the Asian Pacific Regional Aerosol Characterization Experiment, J. Geophys. Res., 110, D14301, doi:10.1029/2004JD005671, 2005.

Han, S., Kondo, Y., Oshima, N., Takegawa, N., Miyazaki, Y., Hu, M., Lin, P., Deng, Z., Zhao, Y., Sugimoto, N., and Wu, Y.: Temporal variations of elemental carbon in Beijing, J. Geophys. Res., 114, D23202, doi:10.1029/2009jd012027, 2009.

Heal, M. R.: The application of carbon-14 analyses to the source apportionment of atmospheric carbonaceous particulate matter: a review, Anal. Bioanal. Chem., 406, 81–98, doi:10.1007/s00216-013-7404-1, 2014.

Heald, C. L., Jacob, D. J., Jones, D. B. A., Palmer, P. I., Logan, J. A., Streets, D. G., Sachse, G. W., Gille, J. C., Hoffman, R. N., and Nehrkorn, T.: Comparative inverse analysis of satellite (MOPITT) and aircraft (TRACE-P) observations to estimate Asian sources of carbon monoxide, J. Geophys. Res., 109, D15S04, doi:10.1029/2004JD005185, 2004.

Hein, R., Crutzen, P. J., and Heimann, M.: An inverse modeling approach to investigate the global atmospheric methane cycle, Global Biogeochem. Cy., 11, 43–76, 1997.

Henze, D. K., Hakami, A., and Seinfeld, J. H.: Development of the adjoint of GEOS-Chem, Atmos. Chem. Phys., 7, 2413–2433, doi:10.5194/acp-7-2413-2007, 2007.

Henze, D. K., Seinfeld, J. H., and Shindell, D. T.: Inverse modeling and mapping US air quality influences of inorganic $PM_{2.5}$ precursor emissions using the adjoint of GEOS-Chem, Atmos. Chem. Phys., 9, 5877–5903, doi:10.5194/acp-9-5877-2009, 2009.

Horvath, H.: Atmospheric light absorption–A review, Atmos. Environ., 27, 293–317, 1993.

Huebert, B. J., Bates, T., Russell, P. B., Shi, G., Kim, Y. J., Kawamura, K., Carmichael, G., and Nakajima, T.: An overview of ACE-Asia: Strategies for quantifying the relationships between Asian aerosols and their climatic impacts, J. Geophys. Res., 108, 8633, doi:10.1029/2003JD003550, 2003.

Intergovernmental Panel on Climate Change (IPCC): Climate Change 2013: The Physical Science Basis, Contribution of Working Group I to the Fifth Assessment Report of the Intergovernmental Panel on Climate Change, edited by: Stocker, T. F., Qin, D., Plattner, G.-K., Tignor, M., Allen, S. K., Boschung, J., Nauels, A., Xia, Y., Bex, V., and Midgley, P. M., Cambridge University Press, Cambridge, United Kingdom and New York, NY, USA, 1535 pp., 2013.

Jacobson, M. Z.: Effects of externally-through-internally-mixed soot inclusions within clouds and precipitation on global climate, J. Phys. Chem., A 110, 6860–6873, doi:10.1021/Jp056391r, 2006.

Jiang, Z., Jones, D. B. A., Kopacz, M., Liu, J., Henze, D. K., and Heald, C.: Quantifying the impact of model errors on top-down estimates of carbon monoxide emissions using satellite observations, J. Geophys. Res., 116, D15306, doi:10.1029/2010JD015282, 2011.

Jiang, Z., Jones, D. B. A., Worden, J., Worden, H. M., Henze, D. K., and Wang, Y.: Regional data assimilation of multispectral MOPITT observations of CO over North America, Atmos. Chem. Phys. Discuss., 15, 5327–5358, doi:10.5194/acpd-15-5327-2015, 2015a.

Jiang, Z., Jones, D. B. A., Worden, H. M., and Henze, D. K.: Sensitivity of top-down CO source estimates to the modeled vertical structure in atmospheric CO, Atmos. Chem. Phys., 15, 1521–1537, doi:10.5194/acp-15-1521-2015, 2015b.

Jin, Y., Randerson, J. T., Faivre, N., Capps, S., Hall, A., and Goulden, M. L.: Contrasting controls on wildland fires in Southern California during periods with and without Santa Ana winds, J. Geophys. Res.-Biogeosci., 119, 432–450, 2014.

Jones, D. B. A., Bowman, K. W., Logan, J. A., Heald, C. L., Liu, J., Luo, M., Worden, J., and Drummond, J.: The zonal structure of tropical O_3 and CO as observed by the Tropospheric Emission Spectrometer in November 2004 – Part 1: Inverse modeling of CO emissions, Atmos. Chem. Phys., 9, 3547–3562, doi:10.5194/acp-9-3547-2009, 2009.

Kopacz, M., Jacob, D. J., Henze, D. K., Heald, C. L., Streets, D. G., and Zhang, Q.: Comparison of adjoint and analytical bayesian inversion methods for constraining Asian sources of carbon monoxide using satellite (MOPITT) measurements of CO columns, J. Geophys. Res., 114, D04305, doi:10.1029/2007JD009264, 2009.

Kopacz, M., Jacob, D. J., Fisher, J. A., Logan, J. A., Zhang, L., Megretskaia, I. A., Yantosca, R. M., Singh, K., Henze, D. K.,

Burrows, J. P., Buchwitz, M., Khlystova, I., McMillan, W. W., Gille, J. C., Edwards, D. P., Eldering, A., Thouret, V., and Nedelec, P.: Global estimates of CO sources with high resolution by adjoint inversion of multiple satellite datasets (MOPITT, AIRS, SCIAMACHY, TES), Atmos. Chem. Phys., 10, 855–876, doi:10.5194/acp-10-855-2010, 2010.

Kopacz, M., Mauzerall, D. L., Wang, J., Leibensperger, E. M., Henze, D. K., and Singh, K.: Origin and radiative forcing of black carbon transported to the Himalayas and Tibetan Plateau, Atmos. Chem. Phys., 11, 2837–2852, doi:10.5194/acp-11-2837-2011, 2011.

Korontzi, S., McCarty, J., Loboda, T., Kumar, S., and Justice, C.: Global distribution of agricultural fires in croplands from 3 years of Moderate Resolution Imaging Spectroradiometer (MODIS) data, Global Biogeochem. Cy., 20, GB2021, doi:10.1029/2005GB002529, 2006.

Langmann, B., Duncan, B., Textor, C., Trentmann, J., van der Werf, G. R.: Vegetation fire emissions and their impact on air pollution and climate, Atmos. Environ., 43, 107–116, 2009.

Lewis, C. W., Klouda, G. A., and Ellenson, W. D.: Radiocarbon measurement of the biogenic contribution to summertime $PM_{2.5}$ ambient aerosol in Nashville, TN, Atmos. Environ., 38, 6053–6061, 2004.

Lin, J.-T., McElroy, M. B., and Boersma, K. F.: Constraint of anthropogenic NO_x emissions in China from different sectors: a new methodology using multiple satellite retrievals, Atmos. Chem. Phys., 10, 63–78, doi:10.5194/acp-10-63-2010, 2010.

Liu, D. C. and Nocedal, J.: On the limited memory BFGS method for large scale optimization, Math. Program., 45, 503–528, doi:10.1007/BF01589116, 1989.

Malm, W. C., Sisler, J. F., Huffman, D., Eldred, R. A., and Cahill, T. A.: Spatial and seasonal trends in particle concentration and optical extinction in the United States, J. Geophys. Res., 99, 1347–1370, 1994.

Mao, Y. H., Li, Q. B., Zhang, L., Chen, Y., Randerson, J. T., Chen, D., and Liou, K. N.: Biomass burning contribution to black carbon in the Western United States Mountain Ranges, Atmos. Chem. Phys., 11, 11253–11266, doi:10.5194/acp-11-11253-2011, 2011.

Mao, Y. H., Li, Q. B., Chen, D., Zhang, L., Hao, W.-M., and Liou, K.-N.: Top-down estimates of biomass burning emissions of black carbon in the Western United States, Atmos. Chem. Phys., 14, 7195–7211, doi:10.5194/acp-14-7195-2014, 2014.

Martin, R. V., Jacob, D. J., Chance, K., Kurosu, T. P., Palmer, P. I., and Evans, M. J.: Global inventory of nitrogen oxide emissions constrained by space-based observations of NO2 columns, J. Geophys. Res., 108, 4537, doi:10.1029/2003JD003453, 2003.

Martin, R. V., Sioris, C. E., Chance, K., Ryerson, T. B., Bertram, T. H., Wooldridge, P. J., Cohen, R. C., Neuman, J. A., Swanson, A., and Flocke, F. M.: Evaluation of space-based constraints on global nitrogen oxide emissions with regional aircraft measurements over and downwind of eastern North America, J. Geophys. Res., 111, D15308, doi:10.1029/2005JD006680, 2006.

McCarty, J. L., Korontzi, S., Justice, C. O., and Loboda, T.: The spatial and temporal distribution of crop residue burning in the contiguous United States, Sci. Total Environ., 407, 5701–5712, doi:10.1016/j.scitotenv.2009.07.009, 2009.

McMurry, P. H., Shepherd, M. F., and Vickery, J. S.: Particulate Matter Science for Policy Makers: A NARSTO Assessment, Cambridge University Press, New York, NY, 2004.

Meirink, J. F., Bergamaschi, P., and Krol, M. C.: Four-dimensional variational data assimilation for inverse modelling of atmospheric methane emissions: method and comparison with synthesis inversion, Atmos. Chem. Phys., 8, 6341–6353, doi:10.5194/acp-8-6341-2008, 2008.

Melillo, J. M., Richmond, T. C., and Yohe, G. W.: Climate Change Impacts in the United States: The Third National Climate Assessment, U.S. Global Change Research Program, 841 pp., doi:10.7930/J0Z31WJ2, 2014.

Müller, J.-F. and Stavrakou, T.: Inversion of CO and NO_x emissions using the adjoint of the IMAGES model, Atmos. Chem. Phys., 5, 1157–1186, doi:10.5194/acp-5-1157-2005, 2005.

Novakov, T., Kirchstetter, T. W., Sinton, J. E., Sathaye, J. A., Ramanathan, V., Hansen, J. E., and Sato, M.: Large historical changes of fossil-fuel black carbon aerosols, Geophys. Res. Lett., 30, 1324, doi:10.1029/2002GL016345, 2003.

Painter, T. H., Flanner, M. G., Kaser, G., Marzeion, B., VanCuren, R. A., and Abdalati, W.: End of the Little Ice Age in the Alps forced by industrial black carbon, Proc. Natl. Aca. Sci., 110, 15216–15221, 2013.

Palmer, P. I., Jacob, D. J., Jones, D. B. A., Heald, C. L., Yantosca, R. M., Logan, J. A., Sachse, G. W., and Streets, D. G.: Inverting for emissions of carbon monoxide from Asia using aircraft observations over the western Pacific, J. Geophys. Res., 108, D218828, doi:10.1029/2003JD003397, 2003.

Park, R. J., Jacob, D. J., Chin, M., and Martin, R. V.: Sources of carbonaceous aerosols over the United States and implications for natural visibility, J. Geophys. Res., 108, D124355, doi:10.1029/2002JD003190, 2003.

Parrington, M., Palmer, P. I., Henze, D. K., Tarasick, D. W., Hyer, E. J., Owen, R. C., Helmig, D., Clerbaux, C., Bowman, K. W., Deeter, M. N., Barratt, E. M., Coheur, P.-F., Hurtmans, D., Jiang, Z., George, M., and Worden, J. R.: The influence of boreal biomass burning emissions on the distribution of tropospheric ozone over North America and the North Atlantic during 2010, Atmos. Chem. Phys., 12, 2077–2098, doi:10.5194/acp-12-2077-2012, 2012.

Paulot, F., Jacob, D. J., Pinder, R. W., Bash, J. O., Travis, K., and Henze, D. K.: Ammonia emissions in the United States, European Union, and China derived by high-resolution inversion of ammonium wet deposition data: Interpretation with a new agricultural emissions inventory ($MASAGE\_NH_3$), J. Geophys. Res. Atmos., 119, 4343–4364, doi:10.1002/2013JD021130, 2014.

Peterson, D. L. and Marcinkowski, K. W.: Recent Changes in Climate and Forest Ecosystems, Climate Change and United States Forests, Springer, Dordrecht, the Netherlands, 57, 3–11, 2014.

Pickett-Heaps, C. A., Rayner, P. J., Law, R. M., Ciais, P., Patra, P. K., Bousquet, P., Peylin, P., Maksyutov, S., Marshall, J., Rödenbeck, C., Langenfelds, R. L., Steele, L. P., Francey, R. J., Tans, P., and Sweeney, C.: Atmospheric CO_2 inversion validation using vertical profile measurements: Analysis of four independent inversion models, J. Geophys. Res., 116, D12305, doi:10.1029/2010JD014887, 2011.

Qian, Y., Gustafson Jr., W. I., Leung, L. R., and Ghan, S. J.: Effects of soot-induced snow albedo change on snowpack and hydrological cycle in western United States based on Weather Research

and Forecasting chemistry and regional climate simulations, J. Geophys. Res., 114, D03108, doi:10.1029/2008JD011039, 2009.

Ramana, M. V., Ramanathan, V., Feng, Y., Yoon, S.-C., Kim, S.-W., Carmichael, G. R., and Schauer, J. J.: Warming influenced by the ratio of black carbon to sulphate and the black carbon source, Nat. Geosci., 3, 542–545, 2010.

Ramanathan, V. and Carmichael, G.: Global and regional climate changes due to black carbon, Nat. Geosci., 1, 221–227, 2008.

Randerson, J. T., van der Werf, G. R., Giglio, L., Collatz, G. J., and Kasibhatla, P. S.: Global Fire Emissions Database, Version 2 (GFEDv2), available at: http://daac.ornl.gov/ (last acess: 2013), Oak Ridge National Laboratory Distributed Active Archive Center, Oak Ridge, Tennessee, USA, 2007.

Randerson, J. T., Chen, Y., van der Werf, G. R., Rogers, B. M., and Morton, D. C.: Global burned area and biomass burning emissions from small fires, J. Geophys. Res., 117, G04012, doi:10.1029/2012JG002128, 2012.

Reche, C., Querol, X., Alastuey, A., Viana, M., Pey, J., Moreno, T., Rodríguez, S., González, Y., Fernández-Camacho, R., de la Rosa, J., Dall'Osto, M., Prévôt, A. S. H., Hueglin, C., Harrison, R. M., and Quincey, P.: New considerations for PM, Black Carbon and particle number concentration for air quality monitoring across different European cities, Atmos. Chem. Phys., 11, 6207–6227, doi:10.5194/acp-11-6207-2011, 2011.

Rodgers, C. D.: Inverse Methods for Atmospheric Sounding: Theory and Practice, World Sci., Singapore, 2000.

Roy, D. P. and Boschetti, L.: Southern Africa validation of the MODIS, L3JRC, and GlobCarbon burned-area products, IEEE Trans. Geosci. Remote Sens., 47, 1032–1044, doi:10.1109/TGRS.2008.2009000, 2009.

Schichtel, B. A., Malm, W. C., Bench, G., Fallon, S., McDade, C. E., Chow, J. C., and Watson, J. G. : Fossil and contemporary fine particulate carbon fractions at 12 rural and urban sites in the United States, J. Geophys. Res., 113, D02311, doi:10.1029/2007JD008605, 2008.

Seinfeld, J. H., Carmichael, G. R., Arimoto, R., Conant, W. C., Brechtel, F. J., Bates, T. S., Cahill, T. A., Clarke, A. D., Doherty, S. J., Flatau, P. J., Huebert, B. J., Kim, J., Markowicz, K. M., Quinn, P. K., Russell, L. M., Russell, P. B., Shimizu, A., Shinozuka, Y., Song, C. H., Tang, Y., Uno, I., Vogelmann, A. M., Weber, R. J., Woo, J.-H., and Zhang, X. Y.: ACE-ASIA-Regional climatic and atmospheric chemical effects of Asian dust and pollution, Bull. Am. Meteorol. Soc., 85, 367–380, 2004.

Shindell, D. T., Levy, H. II, Schwarzkopf, M. D., Horowitz, L. W., Lamarque, J.-F., and Faluvegi, G.: Multimodel projections of climate change from short-lived emissions due to human activities, J. Geophys. Res., 113, D11109, doi:10.1029/2007JD009152, 2008.

Shindell, D., Kuylenstierna, J. C. I., Vignati, E., van Dingenen, R., Amann, M., Klimont, Z., Anenberg, S. C., Muller, N., Janssens-Maenhout, G., Raes, F., Schwartz, J., Faluvegi, G., Pozzoli, L., Kupiainen, K., Höglund-Isaksson, L., Lisa Emberson, L., Streets, D., Ramanathan, V., Hicks, K., Kim Oanh, N. T., George Milly, G., Martin Williams, M., Demkine, V., and Fowler, D.: Simultaneously mitigating near-term climate change and improving human health and food security, Sciences, 335, 183–189, 2012.

Smith, K. R., Jerrett, M., Anderson, H. R., Burnett, R. T., Stone, V., Derwent, R., Atkinson, R. W., Cohen, A., Shonkoff, S. B., Krewski, D., Pope III, C. A., Thun, M. J., and Thurston, G.: Pub-lic health benefits of strategies to reduce greenhouse-gas emissions: health implications of short-lived greenhouse pollutants, Lancet, 374, 2091–2103, 2009.

Spackman, J. R., Schwarz, J. P., Gao, R. S., Watts, L. A., Thomson, D. S., Fahey, D. W., Holloway, J. S., de Gouw, J. A., Trainer, M., and Ryerson, T. B.: Empirical correlations between black carbon aerosol and carbon monoxide in the lower and middle troposphere, Geophys. Res. Lett., 35, L19816, doi:10.1029/2008GL035237, 2008.

Spracklen, D. V., Mickley, L. J., Logan, J. A., Hudman, R. C., Yevich, R., Flannigan, M. D., and Westerling, A. L.: Impacts of climate change from 2000 to 2050 on fire activity and carbonaceous aerosol concentrations in the western United States, J. Geophys. Res., 114, D20301, doi:10.1029/2008JD010966, 2009.

Stavrakou, T., and Müller, J.-F.: Grid-based versus big region approach for inverting CO emissions using Measurement of Pollution in the Troposphere (MOPITT) data, J. Geophys. Res., 111, D15304, doi:10.1029/2005JD006896, 2006.

Subramanian, R., Kok, G. L., Baumgardner, D., Clarke, A., Shinozuka, Y., Campos, T. L., Heizer, C. G., Stephens, B. B., de Foy, B., Voss, P. B., and Zaveri, R. A.: Black carbon over Mexico: the effect of atmospheric transport on mixing state, mass absorption cross-section, and BC/CO ratios, Atmos. Chem. Phys., 10, 219–237, doi:10.5194/acp-10-219-2010, 2010.

Szidat, S., Jenk, T. M., Synal, H.-A., Kalberer, M., Wacker, L., Hajdas, I., Kasper-Giebl, A., and Baltensperger, U.: Contributions of fossil fuel, biomass-burning, and biogenic emissions to carbonaceous aerosols in Zurich as traced by ^{14}C, J. Geophys. Res., 111, D07206, doi:10.1029/2005JD006590, 2006.

Taylor, K. E.: Summarizing multiple aspects of model performance in a single diagram, J. Geophys. Res., 106, 7183–7192, 2001.

van der Werf, G. R., Randerson, J. T., Giglio, L., Collatz, G. J., Kasibhatla, P. S., and Arellano Jr., A. F.: Interannual variability in global biomass burning emissions from 1997 to 2004, Atmos. Chem. Phys., 6, 3423–3441, doi:10.5194/acp-6-3423-2006, 2006.

Vano, J. A., Udall, B., Cayan, D. R., Overpeck, J. T., Brekke, L. D., Das, T., and Lettenmaier, D. P.: Understanding uncertainties in future Colorado River streamflow, Bull. Am. Meteorol. Soc., 95, 59–78, doi:10.1175/BAMS-D-12-00228.1, 2013.

Walker, T., Jones, D. B. A., Parrington, M., Henze, D. K., Murray, L. T., Bottenheim, J. W., Anlauf, K., Worden, J. R., Bowman, K. W., Shim, C., Singh, K., Kopacz, M., Tarasick, D. W., Davies, J., von der Gathen, P., and Carouge, C. C.: Impacts of midlatitude precursor emissions and local photochemistry on ozone abundances in the Arctic, J. Geophys. Res., 117, D01305 doi:10.1029/2011JD016370, 2012.

Wang, J., Xu, X., Henze, D. K., Zeng, J., Ji, Q., Tsay, S.-C., and Huang, J.: Top-down estimate of dust emissions through integration of MODIS and MISR aerosol retrievals with the GEOS-Chem adjoint model, Geophys. Res. Lett., 39, L08802, doi:10.1029/2012GL051136, 2012.

Wang, X., Wang, Y., Hao, J., Kondo, Y., Irwin, M., Munger, J. W., and Zhao, Y.: Top-down estimate of China's black carbon emissions using surface observations: Sensitivity to observation representativeness and transport model error, J. Geophys. Res. Atmos., 118, 5781–5795, doi:10.1002/jgrd.50397, 2013.

Wang, Y., McElroy, M. B., Jacob, D., and Yantosca, R. M.: A nested grid formulation for chemical transport over

Asia: applications to CO, J. Geophys. Res., 109, D22307, doi:10.1029/2004JD005237, 2004.

Wecht, K. J., Jacob, D. J., Wofsy, S. C., Kort, E. A., Worden, J. R., Kulawik, S. S., Henze, D. K., Kopacz, M., and Payne, V. H.: Validation of TES methane with HIPPO aircraft observations: implications for inverse modeling of methane sources, Atmos. Chem. Phys., 12, 1823–1832, doi:10.5194/acp-12-1823-2012, 2012..

Westerling, A. L., Hidalgo, H. G., Cayan, D. R., and Swetnam, T. W.: Warming and earlier spring increase western U.S. forest fire activity, Science, 313, 940–943, doi:10.1126/science.1128834, 2006.

Xu, B., Cao, J., Hansen, J., Yao, T., Joswia, D. R., Wang, N., Wu, G., Wang, M., Zhao, H., Wei Yang, W., Liu, X., and He, J.: Black soot and the survival of Tibetan glaciers, Proc. Natl. Acad. Sci., 106, 22114–22118, 2009.

Xu, X., Wang, J., Henze, D. K., Qu, W., and Kopacz, M.: Constraints on Aerosol Sources Using GEOS-Chem Adjoint and MODIS Radiances, and Evaluation with Multisensor (OMI, MISR) data, J. Geophys. Res., 118, 6396–6413, DOI: 10.1002/jgrd.50515, 2013.

Yue, X., Mickley, L. J., Logan, J. A., and Kaplan, J. O.: Ensemble projections of wildfire activity and carbonaceous aerosol concentrations over the western United States in the mid-21st century, Atmos. Environ., 77, 767–780, 2013.

Yumimoto, K., Uno, I., Sugimoto, N., Shimizu, A., Liu, Z., and Winker, D. M.: Adjoint inversion modeling of Asian dust emission using lidar observations, Atmos. Chem. Phys., 8, 2869–2884, doi:10.5194/acp-8-2869-2008, 2008.

Zhang, L., Jacob, D. J., Kopacz, M., Henze, D. K., Singh, K., and Jaffe, D. A.: Intercontinental source attribution of ozone pollution at western us sites using an adjoint method, Geophys. Res. Lett., 36, L11810, doi:10.1029/2009gl037950, 2009.

Zhang, L., Jacob, D. J., Downey, N. V., Wood, D. A., Blewitt, D., Carouge, C. C., van Donkelaar, A., Jones, D. B. A., Murray, L. T., and Wang, Y.: Improved estimate of the policy relevant background ozone in the United States using the GEOS-Chem global model with $1/2° \times 2/3°$ horizontal resolution over North America, Atmos. Environ., 45, 6769–6776, doi:10.1016/j.atmosenv.2011.07.054, 2011.

Zhang, Y., Jaeglé, L., van Donkelaar, A., Martin, R. V., Holmes, C. D., Amos, H. M., Wang, Q., Talbot, R., Artz, R., Brooks, S., Luke, W., Holsen, T. M., Felton, D., Miller, E. K., Perry, K. D., Schmeltz, D., Steffen, A., Tordon, R., Weiss-Penzias, P., and Zsolway, R.: Nested-grid simulation of mercury over North America, Atmos. Chem. Phys., 12, 6095–6111, doi:10.5194/acp-12-6095-2012, 2012.

Zhu, L., Henze, D. K., Cady-Pereira, K. E., Shephard, M. W., Luo, M., Pinder, R. W., Bash, J. O., and Jeong, G.-R.: Constraining U.S. ammonia emissions using TES remote sensing observations and the GEOS-Chem adjoint model, J. Geophys. Res. Atmos., 118, 3355–3368, doi:10.1002/jgrd.50166, 2013.

Zyrichidou, I., Koukouli, M. E., Balis, D., Markakis, K., Kioutsioukis, I., Poupkou, A., Melas, D., Boersma, K. F., and van Roozendael, M.: Compilation of a NO_x Emission Inventory for the Balkan Region Using Satellite Tropospheric NO_2 Columns, Advances in Meteorology, Climatology and Atmospheric Physics, Springer Berlin Heidelberg, 1265–1271, 2013.